GEOPHYSICS, VOL. 72, NO. 6 (NOVEMBER-DECEMBER 2007); P. B141–B147, 7 FIGS., 2 TABLES.
10.1190/1.2777004

## Case History

# An integrated geophysical approach for imaging subbasalt sedimentary basins: Case study of Jam River basin, India

V. Chakravarthi[1], G. B. K. Shankar[1], D. Muralidharan[1], T. Harinarayana[1], and N. Sundararajan[2]


### ABSTRACT

An integrated geophysical strategy comprising deep electrical resistivity and gravity data was devised to image subbasalt sedimentary basins. A 3D gravity inversion was used to determine the basement structure of the Permian sediments underlying the Cretaceous formation of the Jam River basin in India. The thickness of the Cretaceous formation above the Permian sediments estimated from modeling 60 deep-electric-sounding data points agrees well with drilling information. The gravity effect of mass deficit between the Cretaceous and Permian formations was found using 3D forward modeling and subsequently removed from the Bouguer gravity anomaly along with the regional gravity field. The modified residual gravity field was then subjected to 3D inversion to map the variations in depth of the basement beneath the Permian sediments. Inversion of gravity data resulted in two basement ridges, running almost east to west, dividing the basin into three independent depressions. It was found that the Katol and Kondhali faults were active even during post-Cretaceous time and were responsible for the development of the subsurface basement ridges in the basin. The inferred 3D basement configuration of the basin clearly brought out the listric nature of these two faults. Further, the extension of the Godavari basin into the Deccan syneclise and the fact that the source-rock studies show the presence of hydrocarbons in the Sironcha block in the northern part of the Godavari basin also shed some light on the hydrocarbon potential of the Jam River basin.


## INTRODUCTION

Out of 26 sedimentary basins in India with an onshore and offshore basinal area of 1.78 million km$^2$, only 40% of the area has been explored moderately for hydrocarbon resources and 60% of the area is yet to be explored. Much of west-central India is covered by basalt, which conceals the geology underneath. This province, referred to as the Deccan syneclise (DS), also covers, to varying degrees, the Godavari, Kaladgi, and Bhima basins. The nature of sedimentary fill in these troughs is yet to be confirmed, but at places, extension of these basins is seen around the periphery of the syneclise (Figure 1). The Oil and Natural Gas Corporation Ltd. (ONGC) of India has identified the DS as a potential prospect area for hydrocarbons. The DS is at the knowledge-building stage, and systematic geoscientific input is needed to decipher the stratigraphy, regional configuration, lithofacies, and structural style to comprehend its hydrocarbon potential.

The discovery of commercial oil and gas fields in addition to the coal bed methane in the Gondwana sediments of Permian-Triassic age in the Krishna-Godavari (KG) subbasin, and the fact that source-rock studies show the presence of hydrocarbons in the Sironcha block in the northern part of the Godavari basin, drew the attention of major oil industries to explore and ascertain the natural resources in and around the Jam River basin (JRB) of India where the Godavari basin extends northwest across the DS (Figure 1). Gondwana sediments of Permian-Triassic age are also present in the JRB, concealed under basalts; at a few selected places on the eastern side, they are exposed to the surface as linear patches (Murthy et al., 1986). The Gondwana sediments in turn rest unconformably over the Archaean basement. A limited number of shallow boreholes have been drilled

Manuscript received by the Editor 19 December 2006; revised manuscript received 15 June 2007; published online 18 September 2007.
[1]National Geophysical Research Institute, Hyderabad, India. E-mail: vcvarthi@rediffmail.com; gbkshankar@yahoo.com; muralidharan@ngri.res.in; thari54@yahoo.com.
[2]Osmania University, Centre of Exploration Geophysics, Hyderabad. India. E-mail: sundararajan_n@yahoo.com.

in the JRB (Chakraborti and Mungal, 1995), but no exploratory well has been drilled to depths sufficient to find traces of oil and gas.

Although Pant et al. (1983) have conducted geologic and geophysical surveys in the JRB, the structural configuration of the basement beneath the Permian sediments is yet to be delineated. On the other hand, Sarma et al. (2004) have conducted regional magnetotelluric (MT) surveys in the basin at random intervals along a few selected traverses and have estimated the basement configuration based on 1D and 2D inversion of MT data; however, 3D configuration is yet to be realized.

Unequivocally, we agree that the spatial location of subbasalt targets and geologic translation of geophysical measurements/interpretation still poses a formidable challenge to practicing geophysicists and at times continues to be cumbersome. Imaging subbasalt structures by conventional P-wave seismic survey is often problematic because (1) the high reflectivity at the top of basalt severely impedes penetration of seismic energy into the deeper layers; (2) energy is scattered, particularly the high-frequency component caused by the rugged topography of the basaltic surfaces and the heterogeneity within the basalt caused by successive lava flows (Martini et al., 2001); and (3) extensive peg-leg multiples exist within the stacked

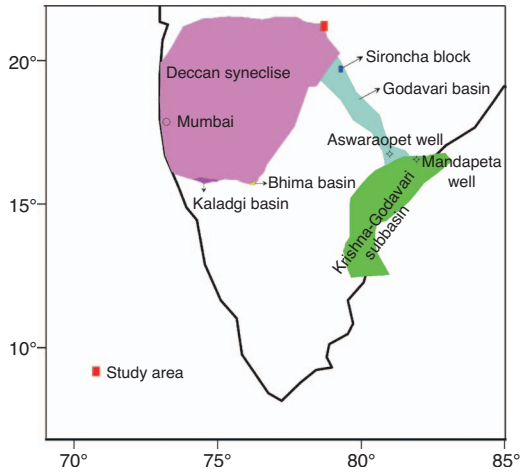


Figure 1. Location map of the Godavari and Jam River basins, India.

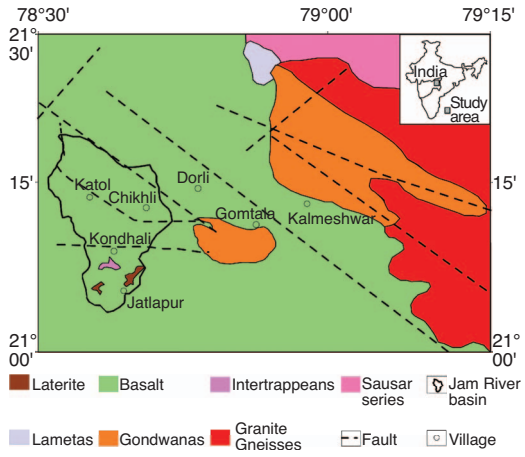


Figure 2. Geology of JRB and adjoining areas. Geological Survey of India topographic sheets 55 K/11 and 55 K/12.

basaltic layers (Satpal et al., 2006). In recent times, geophysical prospecting has moved toward integrating potential fields and electrical methods for regional and prospect evaluation prior to drilling. Such an integrated strategy has proven cost effective for exploration in basalt-covered areas (Prieto et al., 1985; Mitsuhata et al., 1999).

In this direction, deducing some aspects of the earth's subsurface structure on the basis of measurements taken at the surface is invariably an inverse problem. Generally, such inverse problems suffer from an inherent ambiguity or nonuniqueness either during interpretation or toward conclusions. The degree of uncertainty in any geophysical interpretation often can be reduced to an acceptable level by integrating other geophysical field measurements to solve such problems, thereby minimizing or eliminating inherent ambiguity.

The geologic purpose of the integrated study in this paper is to evaluate the 3D configuration of the basement structure of the JRB from integrated modeling of deep-electric-sounding (DES) and gravity data and to investigate the possibilities of hydrocarbon prospects in the basin. This study may find application in hydrocarbon exploration.

## GEOLOGY

The JRB, which covers 400 km$^2$, forms part of the DS and is bounded by 21°02′30″–21°22′30″N latitude and 78°30′00″–78°45′00″E longitude (Figure 2). The northwest strike of the Godavari basin and its extension into the DS has it in close affinity to the depositional sequence of the Gondwana sediments in the JRB (Figure 1). The Godavari basin is filled with a thick pile of sediments of Permian to Recent age, and major oil and gas fields have been discovered in Permian-Jurassic sediments of the basin. A detailed account of the evolutional history, stratigraphy, and oil and gas strikes of the Godavari basin is discussed by Gupta (2006). Further, the upper Kamthi Formation of the JRB has a close affinity to the Permian sediments of the KG basin and hence attracts the attention of the geophysical community for its hydrocarbon potential.

The geology of the JRB and adjoining areas is shown in Figure 2. The topography of the basin is moderate in nature, with the master slope toward the north. The elevation of the topography varies from 200 to 400 m above mean sea level (Figure 3). The Jam River originates near the village of Dhanoli in the southern tip of the basin, flows northward up to Panchdhar, takes a northwest trend up to Digras, and finally flows north-northwestward before joining the Wardha River (Figure 3). The regional stratigraphy of the basin (Mehta et al., 1989) is given in Table 1.

The JRB is covered with flood basalt of Cretaceous-Eocene age. In the southern part of the basin around Jatlapur, 10–12-m-thick laterite occurs as cap rock over the flood basalt (Figure 2). A thin (few meters thick) layer of vesicular/amygdular basalt forms the upper horizon of some of the basalt flows. Vesicular basalts are softer than massive basalts, and vesicles are filled with secondary minerals such as calcite, zeolites, and quartz. Their exposures are seen at the center of the basin, between Katol and Kondhali and also around Chikhli. On the other hand, massive basalts are compact and grayish black, showing a fragmentary structure up to a depth of 1–2 m; they occupy 80%–90% of the area. White, friable limestone intertrappean exposures are seen southwest of Kondhali (Figure 2). Deshmukh et al. (1990) report two prominent faults within the basin, one near Katol and the other near Kondhali (Figure 2).

Based on the structural setting, the basin can be divided into three units (Figure 3): the southern block (between Mendepathar and Dhanoli), the central block (between Mendepathar and Mendhepathar),

and the northern block (between Mendhepathar and the confluence of the Jam River with the Wardha River). The west-northwest–east-southeast strike of the exposed Gondwana sediments on the eastern side of the basin (Figure 2) suggests that these rocks likely extend beneath the basalt flows within the basin (Murthy et al., 1986).

## GEOPHYSICAL SURVEYS

Although many 2D techniques to model basalt-covered areas are available (Prieto et al., 1985; Ferguson et al., 1988), modeling by 3D schemes would be more appropriate because the strike lengths of many sedimentary basins are limited. Based on integrated modeling of deep-resistivity and gravity data, we clarify the 3D basement configuration of the JRB.

Electric and gravity methods measure different rock properties, and each one is more effective when the contrast is significant, although these contrasts may occur at different depths for each method. For example, resistivity data are more sensitive to vertical resistivity changes; in contrast, gravity data are more sensitive to lateral changes in the density of the rock formations. To determine the base of the Permian sediments from gravity anomalies, the base of the basalt needs to be determined using another suitable geophysical method.

In the present case, the thickness of the Cretaceous formation (basalt) over the Permian sediments was estimated by analyzing 60 DES data points, which were supported by drilling. The successful application of DES to explore deep-seated targets is described by Zohdy et al. (1969) and Zohdy (1970). The gravity effect of the mass deficit between basalt and the underlying sediments was computed using a 3D forward-modeling scheme (Chakravarthi et al., 2002) and subsequently was removed from the Bouguer anomalies of the basin along with the regional gravity field. The modified residual gravity anomaly was then modeled using an automated 3D inversion (Chakravarthi, 2003) to configure the basement structure.

## DES DATA ACQUISITION AND PROCESSING

In this direction, as many as 60 DES with a maximum current electrode separation of 1.5–2.0 km using the Schlumberger electrode configuration were conducted in the basin (Figure 3) to identify the basalt-sediment interface. A DC resistivity meter (IGIS model), powered with a 2-kV generator capable of generating a 6-ampere current, was used for the sounding measurements. The effect of lateral inhomogeneities was removed in each sounding (Bhattacharya and Patra, 1968) to attribute the measured signal entirely to vertical distribution of resistivity alone. By and large, sounding curves showing HA (high-low-moderate and very high resistivities), HKH (high-low-moderate-low and high resistivities), and KHK (low-high-low-high and low resistivities) were obtained, indicating the multilayered geoelectric nature of the subsurface.

At the middle of the basin in block 1 (Figure 3), KHK curves were noticed at 27 sounding stations. The descending nature of sounding curves (e.g., DES 37 and DES 35) at larger current electrode separation (Figure 4a) invariably show the presence of low-resistivity Gondwana sediments at depth. In the south, between Mendepathar and Dhanoli (Figure 3), 19 soundings were conducted; they exhibit an ascending trend at larger current electrode separations (Figure 4b). One can note from Figure 4a and b that the behavior of sounding curves at a larger electrode separation at the center could not be seen in the southern block (DES 2 and DES 18), which in turn reveals that a current electrode separation of 2.0 km may be inadequate to receive the signal because of sediments, if any.

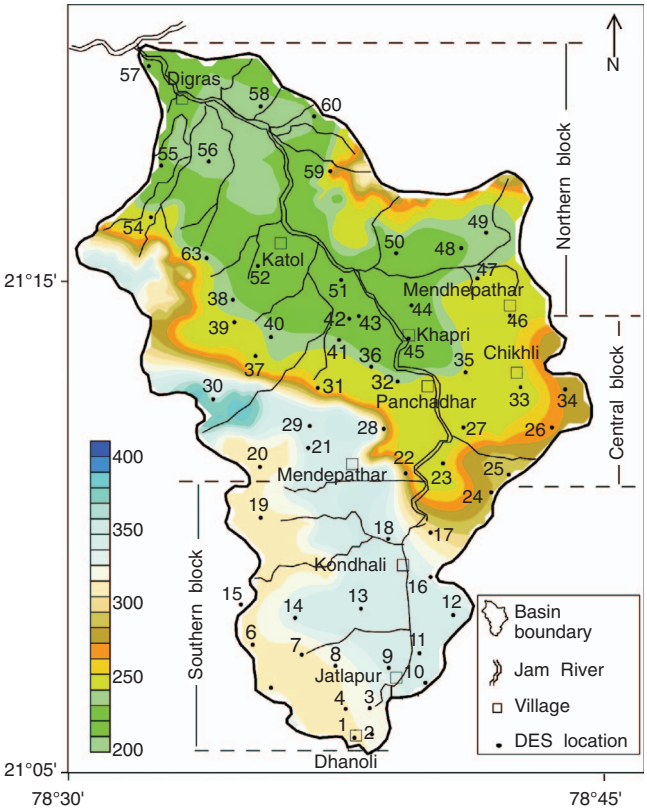


Figure 3. Topographic relief, drainage network, and locations of DES stations.

**Table 1. Regional stratigraphy of Jam River basin, India (after Mehta et al., 1989).**

| Age | Formation | Lithology |
|---|---|---|
| Recent to Quaternary | Alluvium | Black cotton soil, silt, and clay |
| Lower Eocene to upper Cretaceous | Deccan trap | Basaltic flows with intertrappean beds of chert, cherty limestone, and clays |
| | Unconformity | |
| Permian | Lameta beds | Thin sedimentary sequences |
| | Unconformity | |
| Permian to Carboniferous | Gondwana Group | Sandstone (medium to coarse grained) with gritty and conglomeratic bands and intercalated ferruginous shale |
| Archaeans | Granites | Streaky granite gneisses, meta-sediments of Sausar and Sakoli series |

In the northern block (Figure 3), 14 soundings were conducted; some of the typical sounding curves (DES 48 and DES 56) are shown in Figure 4c. The sounding curves in Figure 4c show an increasing trend with the increase of current electrode separation and tend to attain a decreasing trend.

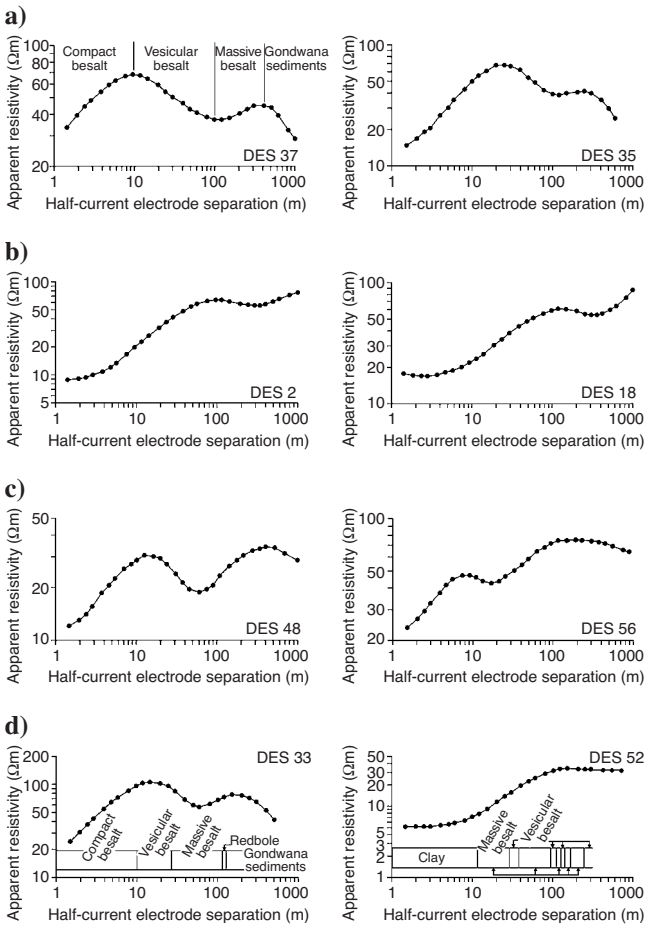


Figure 4. Observed (solid line) and modeled (dotted line) sounding curves. (a) DES 37 and DES 35 in the central block, (b) DES 2 and DES 18 in the southern block, (c) DES 48 and DES 56 in the northern block, and (d) DES 33 and DES 52 at Chikhli and Katol along with the lithological logs.

All of the sounding curves were interpreted in terms of geoelectric parameters (Murakami et al., 1986) such as true resistivity $\rho$ and true thickness of the subsurface $h$; subsequently, two boreholes were drilled: one at Chikhli (DES-33) and the other at Katol (DES-52). At Chikhli, the borehole encountered the Gondwana sediments at a depth of 119 m over a drilled depth of 150 m. At Katol, no sediments were encountered to a drilled depth of 264 m. The lithological sequences and the observed and modeled sounding curves (DES 33 and DES 52) are shown in Figure 4d; the interpreted geoelectrical parameters are given in Table 2. The sounding curve at Chikhli (Figure 4d) clearly shows the presence of sediments beneath the basalt; however, at Katol it is not repeated. The redbole (shaly) formation, which is either infratrappean or the top of clay facies of the Kamthi Formation, is encountered from 109–119 m depth in the borehole at Chikhli. The redbole formation, owing to its relative thickness (Flathe, 1963), could not be identified as an independent geoelectric layer from DES data.

Two additional boreholes were drilled — one nearer to DES 22 and the other just northeast of DES 46 (Figure 3). The thickness of basalt at these two locations was found to be 182 and 107 m against the estimated thickness of 172 and 116 m, respectively. The error between the estimated and actual thickness of basalt for DES 33, DES 22, and DES 46 was found to be 5.9%, 5.5%, and 8.4%, respectively, demonstrating the reliability of DES interpretation.

The interpreted true resistivity of massive basalt is 150–450 Ωm; for vesicular basalt, it is 45 Ωm. At Katol, the resistivity of vesicular and massive basalts together is 55 Ωm. The significant resistivity contrast between the basalt (150–450 Ωm) and the underlying sediments (<20 Ωm) may be attributed to the success of the electric method to delineate the concealed sediments beneath the basalt cover. The resistivities of formations inferred from test soundings (DES 33 and DES 52) are used to constrain the interpretation of other sounding data in the region. The modeled sounding curves in the central, southern, and northern blocks are shown in Figure 4a–c, respectively, and the interpreted geoelectric parameters are given in Table 2.

The thickness of the basalt estimated from interpreting 60 DES data was then used to prepare an isopach (Figure 5a). The thickness of basalt was found to be more than 0.35 km in the northern and

**Table 2. Interpreted geoelectric parameters of deep-electric-sounding (DES) data, Jam River basin, India.**

| DES number | Interpreted true resistivity (Ωm) | | | | | | | Interpreted thickness (m) | | | | | | Thickness of basalt (m) |
|---|---|---|---|---|---|---|---|---|---|---|---|---|---|---|
| | $\rho_1$ | $\rho_2$ | $\rho_3$ | $\rho_4$ | $\rho_5$ | $\rho_6$ | $\rho_7$ | $h_1$ | $h_2$ | $h_3$ | $h_4$ | $h_5$ | $h_6$ | |
| 37 | 37 | 160 | 65 | 33 | 328 | 20 | | 1.95 | 7.82 | 53.82 | 126.82 | 220 | | 346.82 |
| 35 | 20 | 80 | 40 | 350 | 20 | | | 2.1 | 5.4 | 110.0 | 45.0 | | | 162.5 |
| 2 | 9.2 | 18 | 90.2 | 33 | 113 | | | 4.96 | 3.04 | 72.1 | 184.0 | | | 264.1 |
| 18 | 18 | 27 | 90 | 43 | 355 | | | 3.8 | 8.2 | 48.0 | 130.0 | | | 190.0 |
| 48 | 18 | 72 | 21 | 104 | 45 | | | 2.0 | 18.0 | 80.0 | 285.0 | | | 385.0 |
| 56 | 32 | 160 | 23 | 120 | 220 | 35 | 18 | 2.7 | 7.0 | 14.5 | 34.8 | 101 | 70 | 230.0 |
| 33 | 21 | 450 | 45 | 350 | 20 | | | 1.2 | 10.8 | 16.0 | 84.0 | | | 112.0 |
| 52 | 9 | 150 | 55 | 40 | | | | 10.0 | 81.0 | 214.0 | | | | 305.0 |

southern parts of the basin. In general, the thickness of the basalt decreases from both north and south toward the center of the basin. Further, a moat-like depression can be seen at the center of the basin, wherein the thickness of the basalt attains a minimum (<0.1 km). It is also evident from Figure 5a that the sharp gradient in thickness of the basalt between DES 32 and DES 27 and between DES 42 and DES 44 at the center (Figures 3 and 5a) may indicate a fault along which the Jam River apparently flows from south to north. Farther north, the drainage pattern of the river closely follows the trend of the nosing observed in the isopach map of the basalt (Figures 3 and 5a). In short, the thickness of basalt estimated from the interpretation of DES compares well with the borehole information in and around the basin.

## 3D MODELING OF GRAVITY DATA

All gravity corrections, including isostatic correction, were applied to the raw gravity data of the basin, and the resulting Bouguer gravity anomaly was reduced to mean sea level, as shown in Figure 5b (Murthy et al., 1986). A preliminary examination of the gravity data (accuracy of measurements better than 0.2 mGal) indicates that these could provide useful information on the structure of the basin. Despite the fact that the gravity anomaly is very sensitive to near-surface high-density basalt, a large negative gravity anomaly in the basin ($-80$ mGal) suggests that the thickness of concealed sediments is of some significance.

The steep gradient in the anomaly to the south of the circular gravity low (Figure 5b) supports the interpretation that this area is faulted and is quite complex in nature. The Kondhali fault, which was mapped based on geologic studies, coincides with this steep gradient. Further, the nosing of the anomaly along the north-northwest–south-southeast in the southern part of the basin could suggest yet another fault in the basement (Murthy, 1998; Chakravarthi and Sundararajan, 2004). The dislocation of $-82$ mGal along a northwest-southeast trend at the center of the basin is a result of the Katol fault. The thickness of basalt varies quite significantly within the area (Figure 5a); therefore, its gravity effect also varies accordingly. Thus, further processing of the Bouguer gravity anomaly of the area is necessary prior to quantitative interpretation.

In the present study, the regional gravity field was determined by setting the areas of outcropping basement on the eastern side beyond the area of measurement (Figure 2) to be equivalent to 0 mGal. According to Hammer (1963) and Abdoh et al. (1990), to determine the geometry of the base of Permian sediments, the gravity effect of the mass deficit between the basalt and the underlying sediments must be calculated and removed from the Bouguer gravity anomaly along with the regional gravity field. Removing the gravity effect of the mass deficit between basalt and sediments is tantamount to replacing the high-density overburden basalt by a fictitious homogeneous layer with a density akin to that of the underlying sediments. The measured average densities of basalt, Gondwana sediments, and Granite gneisses are given as 2.85, 2.2, and 2.7 g/cm$^3$, respectively.

A rectangular grid with as many as 660 grid nodes — 22 along the east and 30 along the north — was used to approximate the isopach contour map of the basalt (Figure 5a). The grid nodes were selected at an interval of 1.25 km along both the east and north. The gravity effect of the mass deficit between the basalt and sediments was then calculated with a density contrast of 0.65 g/cm$^3$ using the GRAV3DBASE 3D forward-modeling code (Chakravarthi et al., 2002; the code is available at http://www.iamg.org/CGEditor/index.htm in volume 28). The computed gravity effect is shown in Figure 5c. A maximum of an anomalous field of more than 8.5 mGal is observed in the northern and southern blocks (Figure 5c) where the thickness of basalt attains its maximum (Figure 5a).

Removing the regional gravity field and the gravity effect of the mass deficit between the basalt and sediments (Figure 5c) from the Bouguer anomaly (Figure 5b) resulted in the modified residual gravity field (Figure 6a). We observe from the Bouguer (Figure 5b) and modified residual gravity (Figure 6a) fields that (1) the circular gravity low observed in the Bouguer anomaly tends to be elliptical in the modified residual field, with the major axis of the anomaly striking northeast to southwest; (2) trends of gravity lows within the circular anomaly become more pronounced from northwest to southeast; (3) the nosing of the anomaly from north-northwest to south-southeast in the Bouguer anomaly becomes more prominent in the modified residual gravity field; and (4) the significant nosing from east-north-

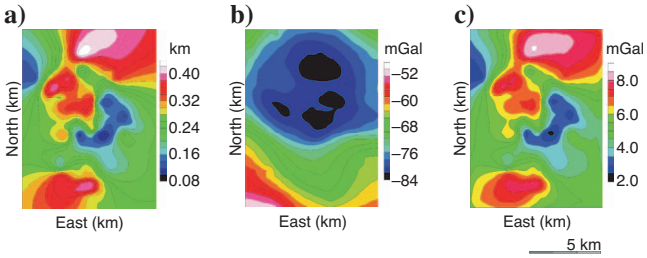


Figure 5. (a) Isopach map of basalt, (b) Bouguer gravity anomaly, and (c) computed gravity effect of the mass deficit between the basalt and underlying sediments.

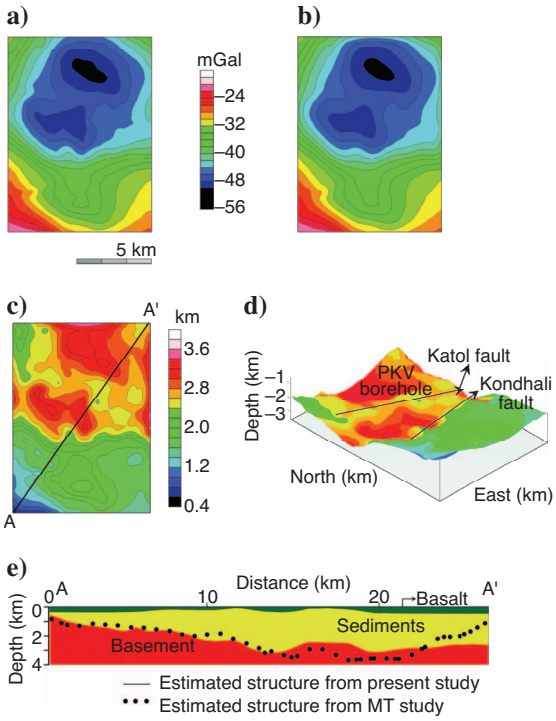


Figure 6. (a) Modified residual gravity anomaly, (b) modeled gravity anomaly subsequent to inversion, (c) plan view of the basement structure, (d) 3D view of the basement structure, and (e) estimated depth from gravity and MT along profile AA′.

east to west-northwest in the southwest part of the basin, which was obscured in the Bouguer anomaly, is seen clearly in the modified residual field.

For quantitative interpretation, the modified residual gravity field of the basin shown in Figure 5a was digitized into 660 grid nodes and inverted using a 3D inversion (Chakravarthi, 2003). The initial depths at all grid nodes were calculated based on the infinite slab formula and subsequently improved using the Marquardt (1963) algorithm (Chakravarthi, 2003). The input to the code consists of the number of grid nodes and grid-node intervals along the north and east, the observed gravity anomaly, and knowledge of the density contrast. The code generates five output files, one with a TXT extension and four with GRD extensions. The output file with a TXT extension provides the interpreted results in ASCII form, but the four output files with a GRD extension contain the information of the observed, modeled gravity anomalies and depth to the basement in a form convenient to view in their respective contour maps using Golden Software's Surfer package. A constant density of $-0.5$ g/cm$^3$ between the sediments and basement was used in the inversion because no density log was available to simulate the variation of density of sedimentary rocks.

The modeled gravity anomaly subsequent to inversion is shown in Figure 6b, and the inferred basement structure in plan and 3D views are shown in Figure 6c and d, respectively. The modeled gravity anomaly in Figure 6b compares well with the observed one (Figure 6a). One can see from Figure 6c and d that the basement deepens toward the north. The Katol and Kondhali faults (Figure 2), which were mapped based on geologic studies (Deshmukh et al., 1990), were revealed clearly in the inferred structural model (Figure 6c and d). A trough-like depression can be seen in the middle of the basin. Two conspicuous basement ridges, running almost east to west, divide the basin into three independent depressions (Figure 6c and d). The subsurface basement ridge in the northern block is controlled by the Katol fault toward the south.

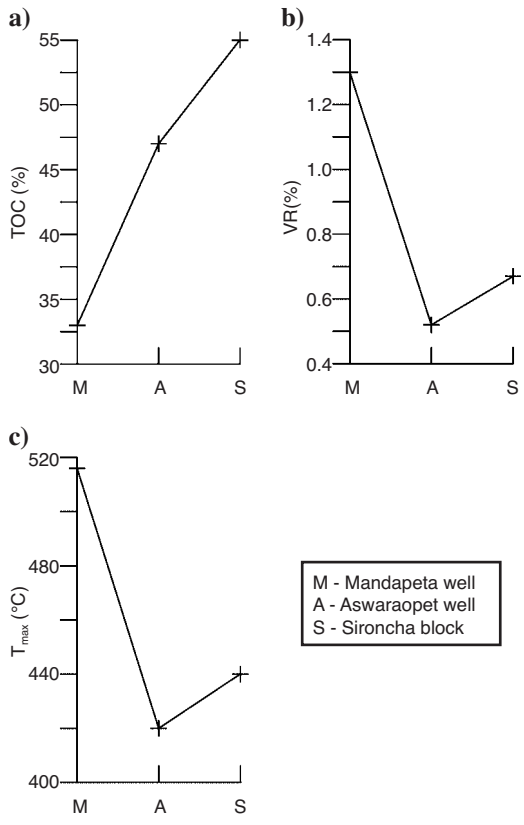


Figure 7. (a) Measured TOC, (b) VR, and (c) $T_{max}$ at Mandapeta well, Aswaraopet well, and Sironcha block in the Godavari basin (B. N. Prabhu, personal communication, 2004; Samanta et al., 1993; Agarwal, 1995).

Figure 6e shows the depth section of the inferred basement from gravity inversion along the profile AA′. The basalt-sediment interface is also plotted along the same profile. The thickness of basalt remains almost the same on either end of the profile except at the center over the basement ridges. This means the basement might have been uplifted subsequent to deposition of the sediments and basalt along the preexisting Katol and Kondhali faults, consequently affecting the thickness of these two. The convex nature of the base of basalt over the subsurface ridges is a testimony to such uplift (Figure 6e).

Further, borehole PKV (Figure 6d), drilled to the south of the basement ridge, has encountered artesian conditions and yields groundwater continuously. Figure 6d reveals that the basement ridge may act as a subsurface barrier to groundwater flow, and the Katol fault (Figure 6d) behaves as a conduit for groundwater movement; hence, artesian conditions are developed in the region. The 3D basement configuration of the basin also brought out the listric nature of the Katol and Kondhali faults (Figure 6d).

The basement configuration derived from MT along the same gravity profile AA′ (Sarma et al., 2004) is also shown in Figure 6e for comparison. The depth sections derived from both gravity and MT surveys compare well with each other with a couple of exceptions. For example, the width of the basement ridge derived from the MT survey from northeast to southwest (Figure 6e) at the center of the basin is much smaller than the corresponding one estimated from gravity data. In addition, the basement structure derived from the MT survey shows an upwarp in the northeastern part (Figure 6e), which is not the case for the gravity survey.

In the present case, the dimensions of the basement ridge derived from gravity data may be more reliable because the gravity anomaly over the ridge shows significant wavelength (Figure 6a). Also, the continuation of a gravity low over and beyond the boundary of the basin in the north, the northwest–southeast-trending major fault in the northern boundary (Figure 2), and the northwest-southeast strike of the exposed Gondwana sediments in the northeastern part beyond the boundary of the basin near Kalmeshwar (Figure 2) support the gravity interpretation that the basement may deepen farther north (Figure 6e). Unlike the gravity case, the MT cross section was prepared by interpolating depth among randomly spaced stations (Sarma et al., 2004) along profile AA′; hence, some features might not be delineated properly. On the other hand, the model estimated from 3D gravity inversion supported by DES data yields a geologically plausible model of the basin.

The maximum depth to the basement at the center and in the northern blocks is in excess of 3.2 km. The thickness of sediments in the Sironcha block in the northern part of the Godavari basin (Figure 1) is about 4.0 km (Agarwal, 1995) and compares well with the estimated thickness of sediments in the JRB. Further, the source-rock studies using comprehensive modern techniques of the organic-rich samples of carbonaceous shales and coal in the Mandapeta and Aswaraopet wells as well as the Sironcha block (Figure 1) show significant quantities of total organic carbon (TOC), vitrinite reflectance (VR), and thermal exposure ($T_{max}$) (Samanta et al., 1993;

Agarwal, 1995; B. N. Prabhu, personal communication, 2004). Figure 7 compares the measured TOC, VR, and $T_{max}$ at Mandapeta and Aswaraopet wells and the Sironcha block. Figure 7a shows that the measured TOC in the Sironcha block exhibits a much higher value than the corresponding ones measured at the Mandapeta and Aswararaopet wells. The measured VR (Figure 7b) and $T_{max}$ (Figure 7c) in Sironcha also show higher values than the Aswaraopet well. Based on the geologic and geochemical studies, Agarwal (1995) shows that the Sironcha block is a potential zone for further exploration of hydrocarbons, which in turn may also shed some light on the hydrocarbon potential of the JRB.

## CONCLUSIONS

Integrated geophysical modeling using deep resistivity and gravity data to decipher the basement configuration of subtrappean sediments is suggested. A 3D configuration of the base of Permian sediments concealed under the Cretaceous formation was inferred from integrated modeling of deep-resistivity and gravity data. The base of the Cretaceous formation was estimated from modeling 60 deep-resistivity sounding data supported by drilling. The gravity effect of the deficit in mass between the Cretaceous and Permian formations was computed in the space domain and then subtracted from the Bouguer gravity anomaly along with the regional field. A 3D inversion of the modified residual gravity resulted in a maximum depth to basement in excess of 3.2 km in the central and northern parts. The faults, which were mapped based on geologic studies, are disclosed well by gravity modeling.

The Katol and Kondhali faults were also active during post-Cretaceous time and might have been responsible for the development of subsurface basement ridges. A basement ridge acting as a subsurface barrier to the flow of groundwater developed artesian conditions at the center of the basin. Generally, the cross section of the estimated structure from gravity data along a southwest–northeast profile compares well with the structural model derived from MT studies. The estimated thickness of sediments in the Sironcha block in the northern part of the Godavari basin compares well with the estimated thickness of the sediments in the JRB. Because the Godavari basin extends further northwest into the DS and also because the source-rock studies of the Sironcha block indicate good source-rock potential for generating hydrocarbons, this study would effectively find application in exploring for hydrocarbons in the JRB.

## ACKNOWLEDGMENTS

The authors sincerely thank associate editor Xiong Li for his many useful suggestions and encouragement. Further, they thank reviewers Patrick S. Millegan, Christine Fichler, Robert Pawlowski, Rao Yalamanchili, and an anonymous reviewer for their appreciations, excellent reviews, and feedback to revise the manuscript as presented. V. P. Dimri, Director, National Geophysical Research Institute, is sincerely thanked for his permission to publish this paper. Chakravarthi acknowledges the Council of Scientific and Industrial Research (CSIR), Government of India, for providing financial assistance under the YS project.

## REFERENCES

Abdoh, A., D. Cowan, and M. Pilkington, 1990, 3D gravity inversion of the Cheshire basin: Geophysical Prospecting, **38**, 999–101.

Agarwal, B. P., 1995, Hydrocarbon prospects of the Pranhita-Godavari graben, India: Petrotech Proceedings, **95**, 115–121.

Bhattacharya, P. K., and H. P. Patra, 1968, Direct current geoelectric sounding: Principles and interpretation: Elsevier Science Publ. Co., Inc.

Chakraborti, R. K., and V. V. Mungal, 1995, Regional exploration by scout drilling for coal in and around Katol area, Nagpur district, Maharashtra: Records of the Geological Society of India, **128**, 239–240.

Chakravarthi, V., 2003, Digitally implemented method for automatic optimization of gravity fields obtained from three-dimensional density interfaces using depth dependent density: U. S. Patent 6 615 139.

Chakravarthi, V., H. M. Raghuram, and S. B. Singh, 2002, 3D forward gravity modeling of density interfaces above which the density contrast varies continuously with depth: Computers & Geosciences, **28**, 53–57.

Chakravarthi, V., and N. Sundararajan, 2004, Ridge regression algorithm for gravity inversion of fault structures with variable density: Geophysics, **69**, 1394–1404.

Deshmukh, S. S., S. M. Godbole, S. Balakrishnan, and A. K. Chatterjee, 1990, Compilation, synthesis and evaluation of available information on all aspects of Deccan traps: Records of the Geological Survey of India, 123, 210–233.

Ferguson, J. F., R. N. Flech, C. L. V. Aiken, J. S. Oldow, and H. Dockery, 1988, Models of the Bouguer gravity and geologic structure at Yucca Flat, Nevada: Geophysics, **53**, 231–244.

Flathe, H., 1963, Five-layer master curvets for the hydrogeological interpretation of geoelectrical resistivity measurements above a two-storey aquifer: Geophysical Prospecting, **11**, 471–508.

Gupta, S. K., 2006, Basin architecture and petroleum system of Krishna Godavari basin, east coast of India: The Leading Edge, **7**, 830–837.

Hammer, S., 1963, Deep gravity interpretation by stripping: Geophysics, **28**, 369–378.

Marquardt, D. W., 1963, An algorithm for least squares estimation of nonlinear parameters: SIAM Journal of Applied Mathematics, **11**, 431–441.

Martini, F., C. J. Bean, S. S. Dolan, and D. Marsan, 2001, Seismic image quality beneath strongly scattering structures and implications for lower crustal imaging: Numerical simulations: Geophysical Journal International, **145**, 423–435.

Mehta, M., 1989, Groundwater resources and development potential of Nagpur district, Maharashtra: Report of Central Groundwater Board, India, 434/DR/12/89.

Mitsuhata, Y., K. Matsuo, and M. Minegishi, 1999, Magnetotelluric survey for exploration of a volcanic-rock reservoir in the Yurihara oil and gas field, Japan: Geophysical Prospecting, **47**, 195–218.

Murakami, Y., A. Zerilli, and R. J. Bisdorf, 1986, A computer program for the automatic inversion of Schlumberger soundings using multi-layer interpretation followed by Dar Zarrouk reduction: USGS Open-File Report OF 86-0288.

Murthy, B. G. K., K. R. Rao, and D. V. Punekar, 1986, Report on the geophysical investigations for delineating Gondwanas below traps in Umrer, Bander, Kamthi and Katol troughs in Nagpur district: Geological Survey of India Deep Geology Project SI/55 KLOP/CR/MH/81/13.

Murthy, I. V. R., 1998, Gravity and magnetic interpretation in exploration geophysics: Geological Survey of India Memoir 40.

Pant, P. R., S. N. Lahiri, A. C. Khare, and R. C. Pathak, 1983, Seismics in exploration for coal — A case study in Kamptee coal field, Maharashtra: Geological Survey of India Special Publication 2, 247–260.

Prieto, C., C. Perkins, and E. Berkman, 1985, Columbia River Basalt plateau: An integrated approach to interpretation of basalt-covered areas: Geophysics, **50**, 2709–2719.

Samanta, U., C. S. Misra, S. Jain, and K. N. Misra, 1993, Organic geochemistry of Gondwana sediments in Pranhita-Godavari grabens: Gondwana Geological Society, 349–361.

Sarma, S. V. S., T. Harinarayana, G. Virupakshi, M. Someswara Rao, Madhusudan Rao, Nandini Nagarajan, T. S. Sastry, and S. Prabhakar E. Rao, 2004, Magnetotelluric investigations in Deccan trap covered areas of Nagpur-Wardha region, India: Journal of Geophysics, **25**, 87–91.

Satpal, O. P. Singh, D. Sar, S. M. Chatterjee, and S. Sawai, 2006, Integrated interpretation for sub-basalt imaging in Saurashtra basin, India: The Leading Edge, **25**, 882–885.

Zohdy, A. A. R., 1970, Mapping basaltic aquifers in southern Idaho by deep electrical soundings: 40th Annual International Meeting, SEG, Expanded Abstracts, M-16.

Zohdy, A. A. R., and D. B. Jackson, 1969, Application of deep electrical soundings for groundwater exploration in Hawaii: Geophysics, **34**, 584–600.